Dynamic Behavior of a Magnetized Multi-Component Hybrid Nanofluid on an Oblique Elongating Interface Affected by Extraction and Permeable Media Interactions

Sidra Ashraf[1]*, Aamir Shahzad[2], Sadia Sher Afzal[3], Asif Arshad[3]
[1]Department of Mathematics, Faculty of Sciences, University of Sargodha, Sargodha, Pakistan
[2]Department of Mathematics, Faculty of Natural Science and Technology, Baba Guru Nanak University, Nankana Sahib, Pakistan
[3]Faculty of Sciences, Superior University Lahore, Lahore, Pakistan
*__Correspondence__: sideeera@gmail.com

Citation | Ashraf. S, Shahzad. A, Afzal. S. S, Arshad. A, "Dynamic Behavior of a Magnetized Multi-Component Hybrid Nanofluid on an Oblique Elongating Interface Affected by Extraction and Permeable Media Interactions", IJIST, Vol. 7, Issue. 4 pp 2928-2939, November 2025
Received | October 17, 2025 **Revised |** November 13, 2025 **Accepted |** November 20, 2025 **Published |** November 27, 2025.

The current study explores the mechanism of heat transfer in non-Newtonian Maxwell tri-component nanofluid flow past an inclined stretching sheet embedded in a permeable medium. The electrically conducting nanofluid is considered under the impact of the Lorentz force. The nanoparticles of three types: Silver, Copper, and Ferric oxide, are considered and mixed with the water taken as a base fluid. The proposed phenomenon in the form of differential equations is solved numerically for the numerical outcomes. These results reflect that the Maxwell fluid parameter has an increasing impact on the velocity of the fluid and a decreasing effect on the temperature. The increasing magnetic force effects highlight the increasing trend in temperature of the fluid and the decreasing impact on the velocity of the fluid. The increasing number of nanoparticles has an increasing thermal effect on the fluid. Similarly, the skin friction and rate of heat transfer are dependent functions of pertinent parameters. The differential equations are solved using the exact solver bvp4c.

Keywords: Nanofluid, Nanoparticles, Magnetized, Permeable Media.

Introduction:

A tri-component hybrid nanofluid is an advanced type of nanofluid formulated by dispersing three distinct nanoparticles into a base fluid, commonly water, ethylene glycol, or kerosene. The nanoparticles may consist of metals, metal oxides, or carbon-based materials like graphene, with each type selected to enhance particular thermal, electrical, or chemical properties.

In practical applications, fluid–surface interactions are often accompanied by mass extraction (suction) and flow through permeable substrates. These mechanisms play a critical role in regulating boundary layer development, stabilizing the flow, and controlling thermal gradients. Additionally, porous media effects are inherent in many natural and engineered systems, including geothermal reservoirs, filtration units, catalytic reactors, and subsurface energy transport devices. The combined influence of permeability, extraction, and magnetic forces introduces complex coupling between momentum, thermal, and mass transport processes that cannot be captured through simplified fluid models.

Motivated by these considerations, the present study investigates the dynamic behavior of a magnetized multi-component hybrid nanofluid flowing over an obliquely elongating interface embedded in a permeable medium. The analysis aims to elucidate the roles of magnetic interaction parameters, multi-nanoparticle composition, extraction intensity, and porous medium permeability on the flow structure and transport characteristics. The outcomes of this work provide insights into the controlled manipulation of hybrid nanofluid systems and contribute to the advancement of efficient thermal and flow control strategies in modern energy and manufacturing technologies.

The Objective of the Study:

The objective of the newly introduced framework is to explore the heat transfer behavior of spherical Ag-Cu-Fe3O4 nanoparticles suspended in water through the application of the MHD Maxwell fluid model. This analysis also examines the impact of stretched inclined surfaces accompanied by suction phenomena within a porous medium. The research involves analyzing various governing factors such as a suction coefficient, permeability factor, magnetic influence, temporal relaxation factor, Maxwell fluid characteristic, and buoyancy effect. The findings from this analysis will carry significant relevance across multiple industrial domains, including thermal energy stations, manufacturing equipment, and the aerospace sector.

The Novelty of the Statement:

The present investigation introduces a newly designed numerical scheme specifically developed to analyze the complex behavior of tri-component hybrid nanofluids within a non-Newtonian Maxwell fluid framework embedded in a permeable medium. The proposed algorithm demonstrates enhanced accuracy, stability, and convergence when compared with existing computational approaches. A key novelty of this work lies in establishing that the inclusion of three distinct nanoparticle constituents significantly improves the rheological performance, heat transfer capability, and flow regulation of Maxwell-type fluids. Compared with existing studies, this work offers a more complete understanding of the underlying physical mechanisms associated with magnetized hybrid nanofluid transport in permeable environments.

Literature Review:

Jalal Mohammed Zayan et al. [1] explored the synthesis and performance evaluation of novel ternary hybrid nanomaterials designed as heat transfer enhancers in H_2O. Farah Nadzirah Jamrus et al. [2] investigated the stability of unsteady flow of a ternary composite nanofluid over a shrinking surface, incorporating the effects of wall mass suction. *A. O.* Akindele et. al. [3] studied the phenomenon of thermal behavior of three-component hybrid nanofluid moving over an inclined magnetized surface illuminated by solar radiation. Prabhu gouda Mallanagouda Patil [4] discussed the transport of a ternary hybrid nanofluid with

Casson-Williamson characteristics over an angled cylinder, considering multiple slip effects. Asad Ullah et al. [5] investigated enhanced heat transfer in a ternary hybrid nanofluid (SiO_2 + Cu + MoS_2/H_2O) under symmetric flow conditions adjacent to a nonlinearly deforming surface. Shilpa Choudhary et. al. [6] describe the thermal behavior of kerosene-based ternary hybrid nanofluids containing two distinct nanoparticle combinations (CNT-Graphene-Fe_3O_4 and MgO-Cu-Au) as they flow across a sheet that stretches in two directions. S. Manjunatha et. al. [7] conduct a theoretical analysis of convective thermal transport in a ternary nanofluid over a deforming sheet. P. Priyadharshini et. al. [8] ternary composite nanofluid dynamics over a symmetrically elongating surface, enhanced via a machine learning prediction technique. Nur Syahirah Wahid et. al. [9] conducted a study about a ternary hybrid nanofluid with first and second-order velocity slips.

Kiran Sajjan et al. [10] conducted the study on the nonlinear transfer of thermal energy regarding a ternary nanofluid passing a Darcy-Brinkman porous framework under a transient heat source/sink. Rupam Shankar Nath and Rudra Kanta Deka [11] presented a simulation-based examination of the behavior of a magnetohydrodynamic tri-nanoparticle suspension fluid (Cu–Al_2O_3–TiO_2/H_2O) flowing over a vertically stretched cylinder within a porous structure influenced by thermal stratification. W. Shinwari et. al. [12] presented the phenomenon of a numerical exploration of the fluid dynamics of water-based triple hybrid nanoparticles over a stretchable bent sheet. Faizan et al. [13] presented a theoretical analysis of ternary hybrid nanofluids within the framework of the Williamson fluid model. Digbash Sahu and Rudra Kanta Deka [14] performed a computational investigation of an MHD tri-nanoparticle suspension fluid (Ag–$CoFe_2O_4$–$ZnO/C_2H_6O_2 + H_2O$) and examined the effect of thermal stratification on a vertically extending cylinder embedded in a permeable medium. Noman Sarwar et. al. [15] carried out the study regarding the implementation of ternary nanoscale particles for heat exchange in a non-Newtonian magnetohydrodynamic fluid system. Ehab A. El-sayed et. al. [16] explained the process of modeling insights into the role of particle shape and enhanced thermal performance in magneto-free convection of a polar tri-hybrid nanofluid around a heat-emitting sphere. Rupam Shankar Nath and Rudra Kanta Deka [17] presented a simulation study of the MHD tri-nanoparticle suspension fluid (Cu − Al_2O_3 − TiO_2/H_2O) in the existence of temperature stratification and radiation effects along a vertically elongated cylinder embedded in a porous medium. Zaheer Abbas et. al. [18] explore the idea regarding the improvement of convective motion in a ternary hybrid nanofluid driven by metachronal propulsion. Vishalakshi A. B. et. al. [19] predict the mechanism of flow of tri-nanoparticle suspension fluid induced by radiative heat transfer and mass transfer over a permeable stretching or contracting surface. Vakapalli Ramu et. al. [20] carried out the study of heat transfer flow of tri-nanoparticle suspension fluid (Al_2O_3-ZrO_2-MgO) over a sinusoidal wavy surface. Hossam A. Nabwey et. al. [21] explored the mechanism of thermal energy transport in magnetohydrodynamic (MHD) flow of Carreau-type ternary hybrid nanofluid across an exponentially stretched curved surface. B.J. Gireesha and L. Anitha [22] examined the impact of shape-dependent ternary hybrid nanoliquid flow through a microchannel, incorporating quadratic radiative heat transfer, with a focus on irreversibility analysis. Javali Kotresh Madhukesh et. al.

[23] explain the process of analysis regarding the heat transfer characteristics of a ternary hybrid nanofluid in a permeable inclined cylinder/plate. Moh Yaseen et. al. [24] presented the idea about the flow of a tri-nanoparticle suspension fluid with gyrotactic microbes across three distinct shapes modeled using the Cattaneo–Christov approach. Khaled Alqawasmi et al. [25] investigated the flow of a ternary hybrid nanofluid over a disk using computational methods, considering nonlinear heat generation and absorption governed by Fourier's heat conduction model.

Mathematical Formulation:

A two-dimensional constant laminar steady fluid flow over a deforming layer with boundary suction in a permeable medium capable of conducting electricity, Maxwell-type viscous tri- component hybrid nanofluid is investigated.

$$\partial x\partial u+\partial y\partial v=0 \quad (1)$$

$$u\partial x\partial u+v\partial y\partial u=\rho thnf\mu thnf(\partial y2\partial 2u+\partial x2\partial 2u)-\rho thnf\beta(u2\partial x2\partial 2u+v2\partial y2\partial 2u+2uv\partial x\partial y\partial 2u)-g\beta thnf(T-T\infty)\sin\phi+\rho thnf\sigma thnfB02u-K0vthnfu \quad (2)$$

$$(\rho Cp)thnf(u\partial x\partial T+v\partial y\partial T)=kthnf\partial y2\partial 2T \quad (3)$$

The above three equations (1) to (3) are subjected to the given constraints.

$$u=Uw(x)=cx,v=-v0,T(x,0)=Tw,C(x,0)=Cwat\ y=0,u\to 0,T\to T\infty,C\to C\infty as\ y\to\infty.(4)$$

Here, the components u and v are the velocity components with horizontal coordinate x and vertical coordinate y, respectively. The symbols of density, kinematic viscosity, dynamic viscosity, heat transfer capability, conductance of electricity, specific heat capacity and heat-induced expansion of tri-component hybrid nanofluid are $\rho thnf$,$vthnf$, $\mu thnf$, $kthnf$, $\sigma thnf$, $(CP)thnf$ and $\beta thnf$ respectively also used in the above model and the involvement of density, kinematic viscosity, dynamic viscosity, heat transfer capability, conductance of electricity, specific heat capacity and heat-induced expansion of base in the governing model are also discussed which are symbolized as ρf,vf, μf, kf, σf , $(CP)f$ and βf respectively. The symbols T, Tw, $T\infty$, C, Cw and $C\infty$ represent the fluid temperature, the heat level at the surface of the flexible sheet, the background assessment of the mean motion-based energy of the particles in a substance, the fluid concentration, the surface concentration, and the concentration in the free stream region, respectively and β, $\boldsymbol{\phi}$, g, $B2$, and K denote the relaxation time constant, the inclination angle of o o the stretching surface, gravitational acceleration, magnetic field intensity, and the permeability constant, respectively.

Solutions Methodology:

In this section, the complete approach used to solve equations (1) to (3) under the conditions of fluid flow specified in Eq. (4) is detailed. The subsequent subsections describe the process by which the partial differential equations (1) to (3) with the flow constraints in equation (4) are transformed into ordinary differential equations (ODEs). Additionally, the method employed to solve the resulting ODE is presented.

Similarity Analysis:

In the following, the similarity transformation provided in (5) will be applied to simplify the set of interconnected and nonlinear partial differential equations (PDEs) shown in (1–3), along with the given constraints specified in (4), into a system of ODEs. We define the corresponding similarity variables as follows.

$$u=cxf'(\eta),v=-cvff(\eta),\ \theta(\eta)=T-T\infty Tw-T\infty,\eta=cvf\ y.(5)\theta(\eta) = \frac{T - T_\infty}{T_w - T_\infty},\ \qquad \eta = \sqrt{\frac{c}{\nu_f}}\, y. \tag{5}\theta(\eta)=Tw-T\infty\ T-T\infty,\eta=vfcy.(5)$$

By using the variables of similarity given in (5) into equations (1-3), the continuity equation is observed to be verified, and the rest of the expressions are expressed as follows;

$$f'''+Aff''-A(f')2+AGr\theta\sin(\Phi)-(M+K)f'=0,(6)$$

$$\theta''+(APr)f\theta'=0.(7)$$

$$f(0)=S,f'(0)=1,\theta(0)=1,f'(\eta)\to 0,\theta(\eta)\to 0as\ \eta\to\infty.(8)$$

Where $A=\frac{-vf}{\ }$ „ $Gr = \frac{g\beta t\underline{hnf}}{\ }\Delta T$ is buoyancy parameter with $\Delta T = (T - T\ \sigma thnf\ B2)$ $M = vthnf\ c2\ w \infty\ \rho thnf\ c$ magnetization parameter, $K = \frac{v_{t\underline{hnf}}}{\ }$ is dimensionless porosity parameter, $Pr = \frac{v_{t\underline{hnf}}}{\ }$ is Prandtl

$c\ K_0$

number with $\alpha = \frac{k_{thnf}}{\alpha_{thnf}}$ as thermal diffusivity, $S = \frac{v_0}{(\rho Cp)_{thnfcvf}}$ is the parameter of suction (vo > 0).

Here, η is basically a variable of similarity, and the prime symbol, ', is the representation of the rate of change w.r.t η.

The relevant physical parameters are the coefficient of skin friction and the Nusselt number, which are expressed as follows

$$\mu_{thnf}\, C_{thnf} = 2\,(\partial u)\,, Nu = -\,x k\,(\partial T)\, f\, \rho_{thnf}\, U2\, \partial y\, x\, k_{ref}\, (Tw - T\infty)\, \partial y\, W\, y=0 \quad y=0 \quad (9)$$

Using (5), in (9), and carrying out some algebraic manipulations, the following modified engineering quantities are obtained

$$\mu_{thnf}\, Re_{1/2} C = 2\, \mu_f\, f''(0)\,, Re_{-1/2} Nu = -\,k_{thnf}\, \theta'(0)\, x\, f\, \rho_{thnf}\, x\, x\, k_{ref}\, \rho_f \quad (10)$$

Where $Re = \frac{cx^2}{v_f}$ Be the Reynolds number. In the following Table 1, water's thermal and physical properties in base fluid role, Fe_3O_4, Ag, and Cu are illustrated.

Table 1. Heat conduction and flow properties

Physical properties	$\rho(Kgm^{-3})$	k (WmK^{-1})	C_p $(JKg^{-1}K^{-1})$	$\sigma(Sm^{-1})$
Base fluid water (H_2O)	997.1	0.613	4179	$5.5x10^{-6}$
$Iron$ (Fe_3O_4)	5180	9.7	670	0.025
Silver (Ag)	10500	429	235	63
$Copper$ (Cu)	8933	401	385	$59.6x10^6$

The equations for the thermophysical features of Ternary Hybrid Nanofluid (THN) are shown below;

$$\rho_{nf} = \rho_f\,(1-\phi 1) + \phi 1(\rho s1)$$

$$\frac{\mu_f}{\mu_{nf}} = (1-\varphi)2.5$$

$$(\rho Cp)_{nf} = (\rho Cp)_f\,(1-\phi 1) + \phi 1\,(\rho Cp)_{s1}$$

$$\frac{k_{nf}}{k_f} = \frac{k_{s1} + 2k_f - 2(k_f - k_{s1})\phi 1}{k_{s1} + 2k_f + \phi 1\,(k_f - k_{s1})}$$

$$\rho_{hnf} = (1-\phi 2)(\rho_f(1-\phi 1) + \phi 1\,\rho s1) + \phi 2\,\rho s2$$

$$\frac{\mu_f}{\mu_{hnf}} = (1-\varphi)2.5(1-\varphi)2.5$$

$$(\rho Cp)_{hnf} = ((1-\phi 2)(\rho Cp)_f\,(1-\phi 1) + \phi 1\,(\rho Cp)_{s1}) + \phi 2\,(\rho Cp)_{s2}$$

$$\frac{k_{hnf}}{k_{nf}} = \frac{k_{s2} + 2k_{nf} - 2(k_{nf} - k_{s2})\phi 2}{k_{s2} + 2k_{nf} + \phi 2(k_{nf} - k_{s2})},$$

$$\rho_{thnf} = (1-\phi 3)[(1-\phi 2)[(1-\phi 1)\rho_f + \phi 1\,\rho s1] + \phi 2\,\rho s2] + \phi 3\,\rho s3$$

$$\frac{\mu_f}{\mu_{thnf}} = (1-\varphi)(1-\varphi)(1-\varphi)2.5(2.5\,3\,2.5$$

$$(\rho Cp)_{thnf} = (1-\phi_3)\left[(1-\phi_2)\left((\rho Cp)_f(1-\phi_1)+\phi_1(\rho Cp)_{s1}\right)+\phi_2(\rho Cp)_{s2}\right]+\phi_3(\rho Cp)_{s3}$$

$$k_{thnf} = k_{s3} + 2k_{hnf} - 2(k_{hnf} - k_{s3})\phi_3 \; k_{hnf} \; k_{s3} + 2k_{hnf} + \phi_3(k_{hnf} - k_{s3}) \quad (11)$$

Where $\phi_1, \phi_2,$ and ϕ_3 are volume fractions of solid nanoparticle Aluminum (Fe_3O_4), Silver (Ag), and Copper (Cu), respectively. Here, 1, $s1$, $s2$, and $s3$ are used to differentiate the thermo-physical properties of the base fluid and nanoparticles of the first kind (Fe_3O_4), second kind (Ag), and third kind (Cu).

Solution Approach:

In equations (6) to (7), together with the given constraints specified in equation (8), are resolved by applying the integrated mathematical solver approach bvp4c. This algorithm operates on the collocation method. Initially, the equations (6-7) along with the given constraints from equation (8) are converted into a system of first-order ODEs and then implemented in MATLAB's bvp4c numerical routine to obtain the solution. The solution procedure is given below:

$$\xi1=f, \xi2=f', \xi3=f'', \xi4=\theta, \xi5=\theta', (12)$$

$$\xi3' = -A\xi1\xi3 + A\xi22 - AGr\xi4\sin(\Phi) + (M+K)\xi2, (13)$$

$$\xi5' = APr\xi1\xi5. (14)$$

$$\xi1(0)=S, \xi2(0)=1, \xi4(0)=1, \xi2(\eta)\to 0, \xi4(\eta)\to 0 \text{ as } \eta\to\infty. (15)$$

Results:

This section presents the numerical outcomes of the governing dimensionless equations describing the magnetized multi-component hybrid nanofluid flow over an oblique elongating interface in a permeable medium with extraction effects. Emphasis is placed on the influence of key control parameters on the velocity and thermal fields, along with associated engineering quantities such as skin friction and heat transfer rate. The impact of the magnetic interaction parameter is observed to suppress the axial velocity throughout the boundary layer. This behavior is attributed to the Lorentz force, which induces resistive drag opposing the fluid motion. Increasing the inclination (obliqueness) parameter enhances flow deceleration near the surface while slightly expanding the momentum boundary layer thickness. In contrast, fluid extraction at the interface significantly reduces the velocity profile and stabilizes the boundary layer, indicating its effectiveness in controlling flow separation. The temperature distribution exhibits a strong dependence on magnetic and porous medium parameters. An increase in magnetic field strength elevates the thermal field due to enhanced Joule heating, resulting in a thicker thermal boundary layer. Conversely, fluid extraction cools the system by drawing heated fluid away from the interface, thereby lowering the temperature profile and improving thermal regulation.

The presence of multi-component nanoparticles significantly enhances thermal transport compared to conventional fluids. The surface shear stress is found to increase with both magnetic and extraction parameters due to enhanced resistance at the fluid–solid interface. However, higher permeability reduces the skin friction coefficient by allowing smoother fluid motion through the porous medium. The local Nusselt number increases notably with extraction and nanoparticle volume fraction, indicating improved heat transfer performance. Magnetic effects slightly reduce the heat transfer rate at elevated field strengths, primarily due to thermal boundary layer thickening.

Overall, the results obtained from the proposed mathematical model are systematically analyzed using the bvp4c numerical solver, which is well known for its accuracy and robustness in handling nonlinear boundary-value problems. The numerical outcomes are presented in both graphical and tabular forms to provide a comprehensive understanding of the flow and heat transfer behavior. The graphical illustrations are employed to examine the variations in the velocity field f' and the temperature distribution θ within the boundary layer, allowing clear visualization of the influence of governing physical parameters on momentum and thermal transport.

In addition, the surface transport characteristics are quantitatively evaluated through tabulated values of the skin friction coefficient $Re^{1/2} C_f$ and the Nusselt number $Re^{-1/2} C_f$. These parameters represent the wall shear stress and the rate of heat transfer at the surface, respectively, and their numerical values facilitate a precise comparison of the effects induced by variations in the controlling parameters.

The computations are carried out for a wide range of physically significant parameters, including the Maxwell fluid parameter β, which characterizes the viscoelastic nature of the fluid; the buoyancy parameter λ, which governs mixed convection effects; the magnetic parameter M, representing the strength of the applied magnetic field; the dimensionless porosity parameter K, accounting for the resistance offered by the porous medium; and the Prandtl number Pr, which reflects the relative influence of momentum and thermal diffusivities. The combined presentation of graphical profiles and numerical tables enables a thorough interpretation of the individual and collective impacts of these parameters on the flow structure and heat transfer performance of the system.

Table 2. Numerical Values of $a)\ Re^{1/2} C_f\ b)\ Re^{-1/2}\ Pr = 7.0,\ M = 1.1;\ B = 0.1, K = 1.1,$

β	$Re^{1/2}\ C_f$	$Re^{-1/2} Nu$
0.1	-3.3496	1,6629
0.3	-3.2477	1.6718
0.5	-3.1623	1.6797
0.7	-3.0893	1.6850

Table 3. Numerical Values of $a)\ Re^{1/2} C_f\ b)\ Re^{-1/2},\ M = 1.1;\ B = 0.1\ , Gr = 0.7, K = 1.1;$

Pr	$Re^{1/2} C_f$	$Re^{-1/2} Nu$
1.0	5.8381	0.0345
5.0	5.8381	0.1959
7.0	5.8379	0.2592
10.0	5.8381	0.3288

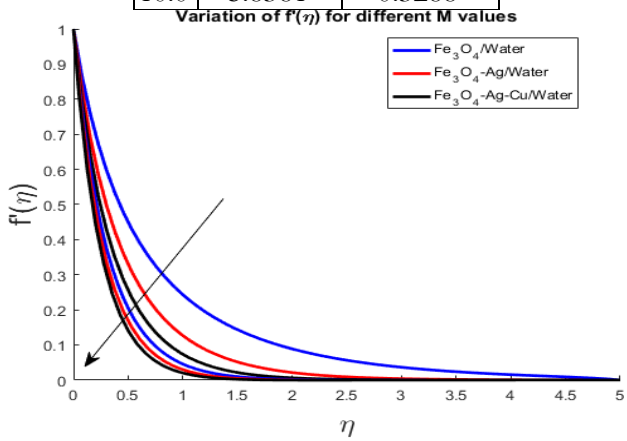

Figure 1. Variation in f' against M Pr=7.0, M=1.1; B = 0.1; Gr=0.1; K = 1.1;

S=0.0;Ec=0.1;L1=0.1; Re=0.1;Rd=1.1;

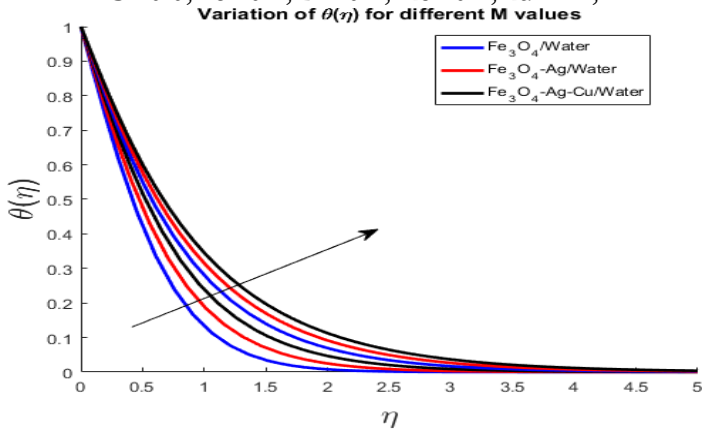

Figure 2. Variation in θ against M Pr=7.0, M=1.1; B = 0.1; Gr=0.1; K = 1.1; S=0.0;Ec=0.1;L1=0.1;Re=0.1;Rd=1.1;

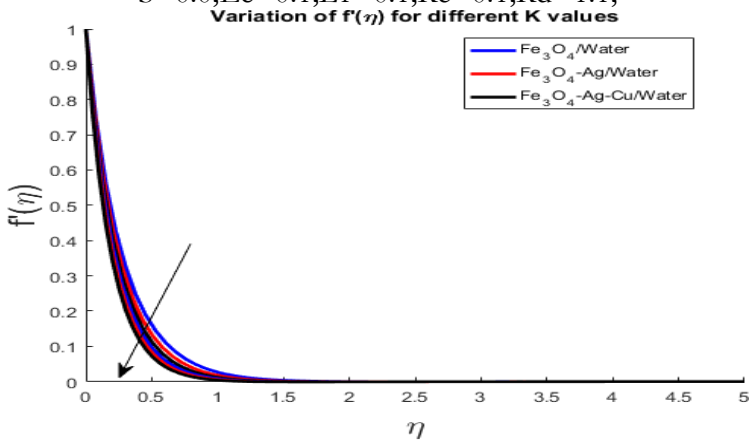

Figure 3. Variation in f' against K Pr=7.0, M=1.1; B = 0.1; Gr=0.1; K = 2.1; S=0.0;Ec=0.1;L1=0.1;Re=0.1;Rd=1.1;

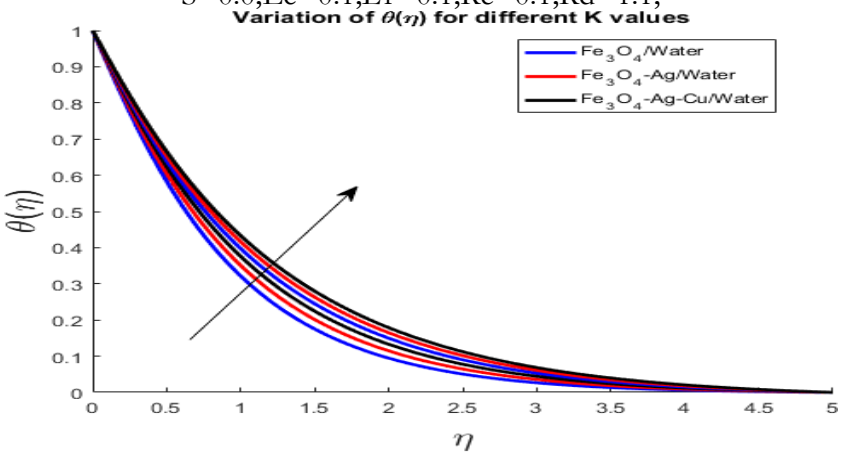

Figure 4. Variation inθ against K Pr=7.0, M=1.1; B = 0.1; Gr=0.1; K = 2.1; S=0.0;Ec=0.1;L1=0.1;Re=0.1;Rd=1.1

Discussion:

Tables 2 and 3 present a comprehensive parametric analysis of the effects of the buoyancy parameter β and the Prandtl number Pr on the skin friction coefficient C_f and the Nusselt number Nu, which characterize surface shear stress and heat transfer performance, respectively. As shown in Table 2, a progressive increase in the buoyancy parameter β results in a noticeable enhancement of the skin friction coefficient. Physically, β quantifies the relative contribution of buoyancy-induced forces arising from temperature gradients within the fluid.

An increase in β strengthens the buoyancy force, which accelerates the fluid motion in the vicinity of the wall and intensifies the velocity gradient at the surface. This amplification of the near-wall velocity gradient leads directly to higher wall shear stress, thereby increasing the skin friction coefficient.

In contrast, the Nusselt number exhibits a decreasing trend with increasing β, indicating a reduction in the rate of heat transfer at the surface. This behavior can be attributed to the thickening of the thermal boundary layer caused by strong buoyancy-driven convection. As buoyancy effects become dominant, thermal energy is redistributed away from the wall region, reducing the temperature gradient at the surface. Since the Nusselt number is directly proportional to the wall temperature gradient, its reduction reflects weakened conductive heat transfer at the interface. Consequently, the relationship between the buoyancy parameter and skin friction is directly proportional, whereas an inverse relationship exists between the buoyancy parameter and the Nusselt number. These findings highlight the dual role of buoyancy forces in enhancing momentum transport while simultaneously suppressing thermal transport, a phenomenon commonly observed in buoyancy-assisted magnetohydrodynamic and nanofluid flow systems.

On the other hand, Table 3 reveals the effects of the Prandtl number. An increase in Pr causes a marginal reduction in skin friction but leads to a notable enhancement in the Nusselt number. Physically, higher Pr values correspond to lower thermal diffusivity, resulting in a thinner thermal boundary layer and improved heat transfer rates. Consequently, the trends associated with Pr are reversed relative to those of the buoyancy parameter, with a direct relationship between Pr and Nu and an inverse association with C_f.

Figures 1 and 2 illustrate the influence of the magnetic parameter M on the velocity and temperature distributions of Fe_3O_4/Water, Ag–Fe_3O_4/Water, and Ag–Cu–Fe_3O_4/Water nanofluids. The results clearly indicate that an increase in MMM leads to a significant suppression of the velocity profile throughout the boundary layer. This reduction in fluid motion is caused by the Lorentz force generated when the electrically conducting nanofluid interacts with the applied magnetic field. The Lorentz force acts as a resistive body force opposing the flow direction, thereby increasing momentum resistance and decelerating the fluid particles near the surface.

Simultaneously, the temperature profile exhibits an increasing trend with higher values of M. The magnetic damping of the velocity field reduces convective heat transport away from the surface, which promotes the accumulation of thermal energy within the boundary layer. In addition, the work done against the Lorentz force enhances viscous dissipation, further contributing to the rise in temperature. This combined effect results in a thicker thermal boundary layer and elevated temperature levels for all considered nanofluids. The influence of the magnetic parameter is more pronounced in hybrid and ternary hybrid nanofluids due to their higher electrical conductivity, which intensifies the magnetic resistance and amplifies thermal energy generation within the flow field.

Similarly, Figures 3 and 4 illustrate the effects of the permeability–magnetic interaction parameter K on the velocity and temperature fields of the considered nanofluids. The results indicate that increasing K leads to a noticeable suppression of the velocity profile and a simultaneous enhancement of the temperature distribution for all nanofluid configurations. Physically, higher values of K represent stronger magnetic resistance and reduced permeability within the porous medium, which intensifies the opposing drag force acting on the fluid. This additional resistance weakens fluid momentum, resulting in a thicker velocity boundary layer and reduced convective transport.

The reduction in fluid motion limits the removal of thermal energy from the surface, thereby thickening the thermal boundary layer and elevating the temperature within the flow domain. A comparative analysis further reveals that Fe_3O_4/Water and Ag–Fe_3O_4/Water

nanofluids maintain relatively higher velocity magnitudes due to their lower effective viscosity and magnetic interaction effects. In contrast, the Ag–Cu–Fe_3O_4/Water nanofluid exhibits the highest temperature levels, which can be attributed to its enhanced thermal conductivity and synergistic nanoparticle interactions that promote heat retention. These findings highlight the critical role of the permeability–magnetic interaction parameter in controlling momentum and heat transfer characteristics in magnetized porous media flows.

Conclusion:

This study has examined the dynamic characteristics of a magnetized multi-component hybrid nanofluid flowing over an oblique elongating interface in the presence of fluid extraction and a permeable medium. A comprehensive mathematical model was formulated to capture the coupled influences of magnetic forces, porous resistance, surface inclination, and multi-component nanoparticle interactions on the momentum and thermal transport processes. By employing similarity transformations and an efficient numerical solution strategy, the governing nonlinear system was solved with a high level of accuracy and stability. The obliqueness of the elongating interface was also observed to markedly influence flow separation tendencies and thermal gradients.

Overall, the present work provides valuable insight into the complex interplay between magnetic effects, porous medium interactions, and multi-component nanoparticle dynamics. The findings offer practical guidance for the design and optimization of advanced thermal management systems, energy transport devices, and magneto-fluidic applications where controlled heat and mass transfer are essential. Future investigations may extend this framework to unsteady flows, non-Newtonian carrier fluids, and variable thermophysical properties to further broaden its applicability.

References:

[1] S. U. S. Choi, "Nanofluids: A new field of scientific research and innovative applications," *Heat Transf. Eng.*, vol. 29, no. 5, pp. 429–431, May 2008, doi: 10.1080/01457630701850778;CTYPE:STRING:JOURNAL.

[2] "New polypyrrole-multiwall carbon nanotubes hybrid materials." Accessed: Dec. 09, 2025. [Online]. Available: https://www.researchgate.net/publication/266224651_New_polypyrrole-multiwall_carbon_nanotubes_hybrid_materials

[3] S. U. S. Choi, S. Li, and J. A. Eastman, "Measuring thermal conductivity of fluids containing oxide nanoparticles," *J. Heat Transfer*, vol. 121, no. 2, pp. 280–289, 1999, doi: 10.1115/1.2825978.

[4] S. K. Das, N. Putra, P. Thiesen, and W. Roetzel, "Temperature Dependence of Thermal Conductivity Enhancement for Nanofluids," *J. Heat Transfer*, vol. 125, no. 4, pp. 567–574, Aug. 2003, doi: 10.1115/1.1571080.

[5] Y. Xuan and W. Roetzel, "Conceptions for heat transfer correlation of nanofluids," *Int. J. Heat Mass Transf.*, vol. 43, no. 19, pp. 3701–3707, Oct. 2000, doi: 10.1016/S0017-9310(99)00369-5.

[6] L. Godson, B. Raja, D. Mohan Lal, and S. Wongwises, "Enhancement of heat transfer using nanofluids—An overview," *Renew. Sustain. Energy Rev.*, vol. 14, no. 2, pp. 629–641, Feb. 2010, doi: 10.1016/J.RSER.2009.10.004.

[7] R. Dharmalingam, K. K. Sivagnanaprabhu, B. Senthil Kumar, and R. Thirumalai, "Nano Materials and Nanofluids: An Innovative Technology Study for New Paradigms for Technology Enhancement," *Procedia Eng.*, vol. 97, pp. 1434–1441, Jan. 2014, doi: 10.1016/J.PROENG.2014.12.425.

[8] "Enhancing thermal conductivity of fluids with nanoparticles." Accessed: Dec. 09, 2025. [Online]. Available: https://www.researchgate.net/publication/236353373_Enhancing_thermal_conducti

vity_of_fluids_with_nanoparticles

[9] M. Nuim Labib, M. J. Nine, H. Afrianto, H. Chung, and H. Jeong, "Numerical investigation on effect of base fluids and hybrid nanofluid in forced convective heat transfer," *Int. J. Therm. Sci.*, vol. 71, pp. 163–171, Sep. 2013, doi: 10.1016/J.IJTHERMALSCI.2013.04.003.

[10] U. Khan, S. Ahmad, A. Hayyat, I. Khan, K. S. Nisar, and D. Baleanu, "On the Cattaneo–Christov Heat Flux Model and OHAM Analysis for Three Different Types of Nanofluids," *Appl. Sci. 2020, Vol. 10, Page 886*, vol. 10, no. 3, p. 886, Jan. 2020, doi: 10.3390/APP10030886.

[11] D. Lu, M. Ramzan, M. Mohammad, F. Howari, and J. D. Chung, "A Thin Film Flow of Nanofluid Comprising Carbon Nanotubes Influenced by Cattaneo-Christov Heat Flux and Entropy Generation," *Coatings 2019, Vol. 9, Page 296*, vol. 9, no. 5, p. 296, May 2019, doi: 10.3390/COATINGS9050296.

[12] M. Abdul Basit, M. Imran, S. A. Khan, A. Alhushaybari, R. Sadat, and M. R. Ali, "Partial differential equations modeling of bio-convective sutterby nanofluid flow through paraboloid surface," *Sci. Reports 2023 131*, vol. 13, no. 1, pp. 6152-, Apr. 2023, doi: 10.1038/s41598-023-32902-z.

[13] T. Oreyeni, A. Oladimeji Akindele, A. Martins Obalalu, S. Olakunle Salawu, and K. Ramesh, "Thermal performance of radiative magnetohydrodynamic Oldroyd-B hybrid nanofluid with Cattaneo–Christov heat flux model: Solar-powered ship application," *Numer. Heat Transf. Part A Appl.*, vol. 85, no. 12, pp. 1954–1972, 2024, doi: 10.1080/10407782.2023.2213837.

[14] A. Asghar *et al.*, "Magnetized mixed convection hybrid nanofluid with effect of heat generation/absorption and velocity slip condition," *Heliyon*, vol. 9, no. 2, Feb. 2023, doi: 10.1016/j.heliyon.2023.e13189.

[15] O. K. Koriko, N. A. Shah, S. Saleem, J. D. Chung, A. J. Omowaye, and T. Oreyeni, "Exploration of bioconvection flow of MHD thixotropic nanofluid past a vertical surface coexisting with both nanoparticles and gyrotactic microorganisms," *Sci. Reports 2021 111*, vol. 11, no. 1, pp. 16627-, Aug. 2021, doi: 10.1038/s41598-021-96185-y.

[16] I. Waini, A. Ishak, and I. Pop, "Hybrid Nanofluid Flow Past a Permeable Moving Thin Needle," *Math. 2020, Vol. 8, Page 612*, vol. 8, no. 4, p. 612, Apr. 2020, doi: 10.3390/MATH8040612.

[17] M. A. Qureshi, "Thermal capability and entropy optimization for Prandtl-Eyring hybrid nanofluid flow in solar aircraft implementation," *Alexandria Eng. J.*, vol. 61, no. 7, pp. 5295–5307, Jul. 2022, doi: 10.1016/J.AEJ.2021.10.051.

[18] A. M. Obalalu *et al.*, "Computational study of Cattaneo–Christov heat flux on cylindrical surfaces using CNT hybrid nanofluids: A solar-powered ship implementation," *Case Stud. Therm. Eng.*, vol. 45, p. 102959, May 2023, doi: 10.1016/J.CSITE.2023.102959.

[19] Z. Xie, J. Jiao, and K. Yang, "Theoretical and experimental study on the fluid-structure-acoustic coupling dynamics of a new water lubricated bearing," *Tribol. Int.*, vol. 177, p. 107982, Jan. 2023, doi: 10.1016/J.TRIBOINT.2022.107982.

[20] T. Hayat, Z. Abbas, and I. Pop, "Mixed convection in the stagnation point flow adjacent to a vertical surface in a viscoelastic fluid," *Int. J. Heat Mass Transf.*, vol. 51, no. 11–12, pp. 3200–3206, Jun. 2008, doi: 10.1016/J.IJHEATMASSTRANSFER.2007.05.032.

[21] N. Balci, B. Thomases, M. Renardy, and C. R. Doering, "Symmetric factorization of the conformation tensor in viscoelastic fluid models," *J. Nonnewton. Fluid Mech.*, vol. 166, no. 11, pp. 546–553, Jun. 2011, doi: 10.1016/J.JNNFM.2011.02.008.

[22] T. Hayat and A. Alsaedi, "On Thermal Radiation and Joule Heating Effects in MHD

Flow of an Oldroyd-B Fluid with Thermophoresis," *Arab. J. Sci. Eng. 2011 366*, vol. 36, no. 6, pp. 1113–1124, Aug. 2011, doi: 10.1007/S13369-011-0066-4.

[23] T. Hayat, M. I. Khan, M. Farooq, A. Alsaedi, and T. Yasmeen, "Impact of Marangoni convection in the flow of carbon–water nanofluid with thermal radiation," *Int. J. Heat Mass Transf.*, vol. 106, pp. 810–815, Mar. 2017, doi: 10.1016/J.IJHEATMASSTRANSFER.2016.08.115.

[24] A. Ishak, Y. Y. Lok, and I. Pop, "Stagnation-point flow over a shrinking sheet in a micropolar fluid," *Chem. Eng. Commun.*, vol. 197, no. 11, pp. 1417–1427, Nov. 2010, doi: 10.1080/00986441003626169;CTYPE:STRING:JOURNAL.

[25] R. Ali, M. I. Asjad, A. Aldalbahi, M. Rahimi-Gorji, and M. Rahaman, "Convective flow of a Maxwell hybrid nanofluid due to pressure gradient in a channel," *J. Therm. Anal. Calorim. 2020 1432*, vol. 143, no. 2, pp. 1319–1329, Oct. 2020, doi: 10.1007/S10973-020-10304-X.